Stein Variational Online Changepoint Detection with Applications to Hawkes Processes and Neural Networks

Gianluca Detommaso [1] Hanne Hoitzing [1] Tiangang Cui [2] Ardavan Alamir [1]

Abstract

Bayesian online changepoint detection (BOCPD) (Adams & MacKay, 2007) offers a rigorous and viable way to identity changepoints in complex systems. In this work, we introduce a Stein variational online changepoint detection (SVOCD) method to provide a computationally tractable generalization of BOCPD beyond the exponential family of probability distributions. We integrate the recently developed Stein variational Newton (SVN) method (Detommaso et al., 2018) and BOCPD to offer a full online Bayesian treatment for a large number of situations with significant importance in practice. We apply the resulting method to two challenging and novel applications: Hawkes processes and long short-term memory (LSTM) neural networks. In both cases, we successfully demonstrate the efficacy of our method on real data.

1. Introduction

In most applied sciences and real-life scenarios, the ability to promptly detect and react to sudden changes is extremely desirable. Examples of current applications include hedge coverage in financial trading, attack detection in cybersecurity, prediction of natural disasters, and many others. In statistical analysis, the attempt to identify these changes is called *changepoint detection*.

Methods that fall under this category try to simultaneously minimize the following three important metrics: i) false negative rate, ii) false positive rate and iii) detection delay. False negatives must be avoided at any cost: missing the occurrence of an earthquakes could be fatal for thousands of people; ignoring a cyber-attack could incur huge losses. Similarly, avoiding false positives has significant importance: too many alerts will hide 'true' changes, leading the analyst to underestimate important information and to lose confidence in the statistical methodology. Finally, most applications require a realtime reaction once new data is observed. Online algorithms should minimize detection delay, yet without undermining the first two metrics.

Among the literature in changepoint detection, probabilistic approaches have gained popularity for their ability to predict both the next observation and its uncertainty in an online fashion. Among the algorithms following a probabilistic approach, one that has significantly characterized the field for its simplicity and efficacy is *Bayesian online changepoint detection* (BOCPD) (Adams & MacKay, 2007). In its original formulation, this method exploits conjugate priors to construct predictive models in closed form to quickly assess whether a changepoint has occurred. Although conjugate priors constitute an ingenious tool to decrease detection delay, their simplicity also represents their major limitation: whenever the data substantially differ from the simple model in use, false negative and false positive rates are very large.

Several Bayesian inference methods have been proposed to extend BOCPD to non-conjugate scenarios (Niekum et al., 2015; Mavrogonatou & Vyshemirsky, 2016; Saatçi et al., 2010; Turner et al., 2013). Although these methods form major contributions and have their own strengths, they also come with natural weaknesses: Markov chain Monte Carlo is not fast in online situations; posterior approximations through variational inference might be far from the real ones; Gaussian processes struggle for long time series and suffer in high-dimension; sequential Monte Carlo has degeneracy problems in high-dimension.

In this work, we propose a *Stein variational online changepoint detection* (SVOCD) method, a combination of BOCPD and Stein variational inference (Liu & Wang, 2016). Stein variational inference is a cutting-edge Bayesian inference methodology that transports, sequentially and deterministically, a set of particles towards a posterior probability density. The advantage of SVOCD compared to the extensions mentioned above is twofold: i) rather than merely approximating the posterior density, the empirical density represented by the particles asymptotically converges to the posterior density as the number of particles increases (Liu,

[1]InfoSec division, G-Research, London (UK) [2]School of Mathematical Sciences, Monash University, Melbourne (Australia). Correspondence to: Gianluca Detommaso <detommaso.gianluca@gmail.com>.

2017), ii) rather than re-computing the posterior density from scratch when new data becomes available, it can be updated quickly which is crucial for online applications. Quick updates are possible because the posterior density can be used as the initial particle density to infer the next posterior density as new data points arrive. Assuming the true posterior does not change massively, the particle locations can be adjusted with just a few iterations. As a Stein variational algorithm we adopt Stein variational Newton (SVN), which was shown to drastically improve convergence speed and scalability to high-dimension compared to Stein variational gradient descent (SVGD) (Detommaso et al., 2018).

Additionally, we successfully apply our methodology to two complex models which represent a large number of real-life scenarios and which currently lack a rigorous Bayesian changepoint analysis.[1] First, we apply SVOCD to Hawkes processes. Hawkes processes are an interesting example of point processes for which the intensity increases with the occurrence of an event and exponentially decays over time. They are very flexible, can describe many self-exciting situations, and have been used in a wide range of applications, e.g. finance (Embrechts et al., 2011; Bacry et al., 2015), social networks (Zhou et al., 2013), cybersecurity (Price-Williams & Heard, 2017), earthquakes (Ogata, 1998), and criminality (Lewis et al., 2012). To the best of our knowledge, this is the first attempt to perform online changepoint detection on Hawkes process in a fully Bayesian fashion. We successfully show how this can be done using SVOCD.

Secondly, we study the combination of BOCPD with a Bayesian *long short-term memory* (LSTM) neural network model. In many situations, there exists no obvious model to describe the evolution of data. LSTM constitutes a great flexible modelling tool which can be trained to describe a specific sequence of data points and predict future points. However, the absence of an explicitly defined model structure can lead to large computational costs: besides a clever architecture, LSTM's descriptive power comes from overparametrization, which makes the training computationally intensive and likely to end up in local minima or flat regions of the parameter space. In this paper, we attempt to overcome these issues by combining a Bayesian formulation of LSTM with BOCPD and train the model using SVN to effectively detect changepoints.

A major contribution of this work is that we integrate the state-of-the-art BOCPD and Stein variational inference to offer a full Bayesian approach for online changepoint detection in general models. The resulting SVOCD can quickly update posterior densities which is of great importance for online applications. We show that our method can be successfully applied to complex models such as Hawkes processes and Bayesian LSTMs. In both cases, our method produces less false positives and requires less iterations compared to other state-of-the-art methods.

The paper is structured as follows: Section 2 describes the background of BOCPD and SVN, and then presents SVOCD. In Sections 3 and 4, we apply SVOCD to Hawkes processes and LSTM, respectively. A conclusion is stated in section 5.

2. Stein variational online changepoint detection

In this section, we will introduce Stein variational online changepoint detection (SVOCD). SVOCD generalizes Bayesian online changepoint detection to probability distributions beyond the exponential family by using the Stein variational Newton method to perform online inference.

2.1. Bayesian online changepoint detection

Suppose we can sequentially observe data points $y_{1:m}$, where the subscript denotes the observation time. Assuming that each observation y_i depends on some model driven by a hidden parameter $\theta \in \mathbb{R}^d$, changepoint detection aims to identify abrupt changes in the parameter θ that produces the observed process. We denote a *changepoint* by a time index $\tau > 1$ at which the abrupt change in θ occurs. Here, we will focus on online changepoint detection. That is, given past observations $y_{1:m}$, we want to detect whether the parameter θ at time $m+1$ is the same as the one at time m. When the new data observed at time $m+1$ becomes available, we want to perform this task recursively.

Bayesian online changepoint detection (BOCPD) has been introduced in (Adams & MacKay, 2007) as a probabilistic approach for online detection of changepoints in a time series. The algorithm has pioneered a considerable amount of interesting follow-up work. Here we provide a description of the general formulation of BOCPD.[2] BOCPD adopts the following reasonable assumption.

A1. Observed data before and after changepoints are independent. That is, y_i is independent of y_j if there exists a changepoint τ such that $i < \tau \leq j$. This way, the dynamics of the underlying system after a changepoint is not affected by what happened before the changepoint.

Let us define $\tau_{m+1} \in \{1, \dots, m+1\}$ to be the changepoint indicator at time $m+1$ which records the time of the occurrence of the last changepoint. The case $\tau_{m+1} = 1$ indicates there has been no changepoint up until time $m+1$. Although a priori τ_{m+1} can assume any value between 1 and $m+1$, in practice one should consider pruning the possible set of

[1]Open source code is available at the GitHub repository gianlucadetommaso/Stein-variational-samplers.

[2]We adopt a formulation without the concept of *run length* in the standard BOCPD, however the method is equivalent.

changepoints according to their posterior probability for significant computational speed-ups (Turner et al., 2009).

Predictive posterior. Suppose we have observed $y_{1:m}$ and we want to detect whether y_{m+1} is a changepoint. For this purpose, we introduce the predictive posterior density $p(y_{m+1}|y_{1:m})$, which measures the probability that y_{m+1} is observed given $y_{1:m}$. However, because of assumption **A1**, y_{m+1} is only dependent on observations since the last changepoint τ_{m+1}. Then, if we define $Y_{\tau_{m+1}} := \{\tau_{m+1}, y_{\tau_{m+1}:m}\}$ to be the information set given by both the changepoint τ_{m+1} and the sequence of observed data points $y_{\tau_{m+1}:m}$ (we define $y_{m+1:m} = \emptyset$), we can marginalize the predictive posterior density as follows:

$$p(y_{m+1}|y_{1:m}) = \sum_{\tau_{m+1}=1}^{m+1} p(y_{m+1}|Y_{\tau_{m+1}})\, p(\tau_{m+1}|y_{1:m})\,. \quad (1)$$

We will now analyse the two factors on the right-hand-side of equation (1).

Predictive model. $p(y_{m+1}|Y_{\tau_{m+1}})$ denotes the predictive probability given the last changepoint τ_{m+1}. By marginalising y_{m+1} over the hidden parameter θ, we can write

$$p(y_{m+1}|Y_{\tau_{m+1}}) = \int p(y_{m+1}|Y_{\tau_{m+1}},\theta)\, p(\theta|Y_{\tau_{m+1}})\, d\theta, \quad (2)$$

where $p(\theta|Y_{\tau_{m+1}})$ denotes the posterior distribution of θ and we refer to $p(y_{m+1}|Y_{\tau_{m+1}},\theta)$ as the *predictive likelihood*.

In original BOCPD, the authors exploit conjugate priors for exponential families of probability distributions to express the predictive density (2) in closed form. Although this approach minimizes changepoint detection delay, for many practical applications the true negative and false positive metrics are compromised because the model is too simplistic to adequately represent complex real-life scenarios. In section 2, we will generalize BOCPD to non-exponential families of probability distributions by introducing Stein variational Newton. This method will enable us to accurately approximate $p(y_{m+1}|Y_{\tau_{m+1}})$ for more complex model choices that can better represent the data and their changepoints, while keeping the detection delay small.

Changepoint posterior. $p(\tau_{m+1}|y_{1:m})$ denotes the posterior probability of the changepoint indicator τ_{m+1}. Using an approach analogous to (Adams & MacKay, 2007), it is easy to show that the joint probability of τ_{m+1} and $y_{1:m}$ can be recursively expressed as

$$p(\tau_{m+1}, y_{1:m}) = \sum_{\tau_m=1}^{m} p(y_m|Y_{\tau_m})\, p(\tau_{m+1}|\tau_m)\, p(\tau_m, y_{1:m-1}). \quad (3)$$

Hence, the joint density on the left-hand-side of (3) can be evaluated by a forward message-passing algorithm which stores the joint density evaluations at the previous iteration and updates them accordingly. The posterior density can then be recovered by normalizing the joint density via $p(y_{1:m}) = \sum_{\tau_{m+1}=1}^{m+1} p(\tau_{m+1}, y_{1:m})$. Note that, given τ_m, we can only have either $\tau_{m+1} = \tau_m$ if y_{m+1} follows the same dynamics as y_m, or $\tau_{m+1} = m+1$ if $m+1$ is a changepoint. Then, we define the *changepoint prior* density

$$p(\tau_{m+1}|\tau_m) = \begin{cases} H_m & \text{if } \tau_{m+1} = m+1\,, \\ 1 - H_m & \text{if } \tau_{m+1} = \tau_m\,, \end{cases} \quad (4)$$

where H_m can be interpreted as a *hazard rate*. Hence, whenever $\tau_{m+1} \neq m+1$, the sum over τ_m in (3) reduces to a single term with $\tau_m = \tau_{m+1}$.

2.2. Stein variational Newton

Consider an intractable target density π on $\mathbb{R}^d$ that we wish to approximate via an empirical measure or, equivalently, a collection of particles. Given a set of particles $(\theta^{(k)})_{k=1}^{N_\theta}$ characterizing an initial reference density q_0, we seek a transport map $T : \mathbb{R}^d \to \mathbb{R}^d$ such that $T_* q_0$, the push-forward map of q_0 through T, is a close approximation of π.[3] Such a map T is not unique: there exist an infinite number of such maps that can serve the purpose (Villani, 2008). In the following, we construct T as a composition of simple maps T_l which are iteratively applied on reference densities q_l such that $q_{l+1} = T_{l*} q_l$. We define each T_l as a perturbation Q_l of the identity map:

$$T_l(\theta) = \theta + Q_l(\theta)\,. \quad (5)$$

When applied to the current reference density q_l, equation (5) defines the push-forward measure $T_{l*} q_l$ as an update of q_l itself along the direction Q_l. The latter will be taken along a vector-valued *Reproducing Kernel Hilbert Space* (RKHS) $\mathcal{H}^d \simeq \mathcal{H} \times \cdots \times \mathcal{H}$ characterized by a kernel $k(\cdot,\cdot)$.

A variational approach. We define the functional

$$Q \mapsto J_{q_l}[Q] := \mathcal{D}_{\text{KL}}((I+Q)_*\, q_l \,||\, \pi)\,, \quad (6)$$

with $Q \in \mathcal{H}^d$. $J_{q_l}[Q]$ measures the Kullback-Leibler (KL) divergence $\mathcal{D}_{\text{KL}}$ between the push-forward map of q_l, along the direction Q, and π. Thus, we want to find a map Q_l such that $J_{q_l}[Q_l] < J_{q_l}[\mathbf{0}]$, where $\mathbf{0}(\theta) = 0$ denotes the zero map. In other words, we are constructing a sequence of densities $q_0, q_1, q_2, \ldots$ that weakly converges to π (see (Liu, 2017) for convergence results).

In order to construct an appropriate map $Q_l \in \mathcal{H}^d$, we define the first variation of J_{q_l} at $S \in \mathcal{H}^d$ along $V \in \mathcal{H}^d$ as

$$DJ_{q_l}[S](V) := \lim_{\tau \to 0} \frac{1}{\tau}\big(J_{q_l}[S + \tau V] - J_{q_l}[S]\big)\,. \quad (7)$$

[3] If T is an invertible map, the push-forward map is defined by $T_* q(\theta) = q(T^{-1}(\theta))\,|\det(\nabla_\theta T(\theta))|$.

Assuming the objective function $J_{q_l} : \mathcal{H}^d \to \mathbb{R}$ is Fréchet differentiable, the *functional gradient* of J_{q_l} at $S \in \mathcal{H}^d$ is the element $\nabla J_{q_l}[S] = (\partial_j J_{q_l}[S])_{j=1}^d$ of $\mathcal{H}^d$ such that

$$DJ_{q_l}[S](V) = \langle \nabla J_{q_l}[S], V\rangle_{\mathcal{H}^d} \quad \forall V \in \mathcal{H}^d\,, \tag{8}$$

where $\langle f, g\rangle_{\mathcal{H}^d} := \sum_{j=1}^d \langle f_j, g_j\rangle_{\mathcal{H}}$ defines an inner product for each $f, g \in \mathcal{H}^d$.

We can also define the second variation of J_{q_l} at S along the pair of directions $V, W \in \mathcal{H}^d$ as

$$D^2 J_{q_l}[S](V,W) := \lim_{\tau\to 0} \frac{DJ_{q_l}[S+\tau W](V) - DJ_{q_l}[S](V)}{\tau}\,. \tag{9}$$

Assuming second-order Fréchet differentiability of J_{q_l}, the *functional Hessian* of J_{q_l} at $S \in \mathcal{H}^d$ is the element $\nabla^2 J_{q_l}[S] = (\partial_i\partial_j J_{q_l}[S])_{i,j=1}^{d,d} \in \mathcal{H}^{d\times d}$ such that

$$D^2 J_{q_l}[S](V,W) = \left\langle \begin{bmatrix} \langle \partial_1 \nabla J_{q_l}[S], W\rangle_{\mathcal{H}^d} \\ \vdots \\ \langle \partial_d \nabla J_{q_l}[S], W\rangle_{\mathcal{H}^d} \end{bmatrix}, V \right\rangle_{\mathcal{H}^d}\,. \tag{10}$$

By combining the results in (Liu & Wang, 2016; Detommaso et al., 2018), we have the following theorem.

Theorem 1 *With the notation above, we have*

$$\begin{aligned} \nabla J_{q_l}[\mathbf{0}](\phi) = -\mathbb{E}_{\theta\sim q_l}[&\nabla_\theta \log\pi(\theta) k(\theta,\phi) \\ &+ \nabla_\theta k(\theta,\phi)]\,, \end{aligned} \tag{11}$$

$$\begin{aligned} \nabla^2 J_{q_l}[\mathbf{0}](\phi,\psi) = \mathbb{E}_{\theta\sim q_l}[&-\nabla_\theta^2 \log\pi(\theta) k(\theta,\phi) k(\theta,\psi) \\ &+ \nabla_\theta k(\theta,\phi)\nabla_\theta k(\theta,\psi)^\top]\,. \end{aligned} \tag{12}$$

Newton method. Given the first and second variations (7)-(9), we can employ a Newton method in function space to sequentially minimize local quadratic approximations of J_{p_l}. The transport map $Q_l \in \mathcal{H}^d$ that minimizes this quadratic form defines the Newton direction and is characterized by the first order stationarity conditions

$$D^2 J_{p_l}[\mathbf{0}](V,W) = -DJ_{p_l}[\mathbf{0}](V)\,, \quad \forall V \in \mathcal{H}^d\,. \tag{13}$$

By combining (8), (10) and Theorem 1, we can formulate *Stein variational Newton*: a non-parametric, second-order optimization method that sequentially pushes forward a set of particles towards the target density π. Several possibilities are now available, including standard Newton, inexact and Quasi-Newton, Newton-CG and trust-region.

Practically, for any Newton-type iteration we need a positive-definite approximation H of $\nabla^2 J_{q_l}[\mathbf{0}]$. To obtain this, it is sufficient to construct a positive-definite approximation $H_\pi \approx -\nabla^2 \log\pi$, and define a matrix H as follows:

$$\begin{aligned} H(\phi,\psi) = \mathbb{E}_{\theta\sim q_l}[&H_\pi(\theta) k(\theta,\phi) k(\theta,\psi) \\ &+ \nabla_\theta k(\theta,\phi)\nabla_\theta k(\theta,\psi)^\top]\,. \end{aligned} \tag{14}$$

Algorithm 1 describes an inexact Newton method with a block-diagonal approximation of the Hessian, which was shown in (Detommaso et al., 2018) to converge quickly and accurately. Both expectation operators in (11) and (14), which appear in Algorithm 1, are taken with respect to the empirical density q_l characterized by a set of particles $(\theta_l^{(k)})_{k=1}^{N_\theta}$. Hence, for any function $f : \mathbb{R}^d \to \mathbb{R}$, we can write the expectation as $\mathbb{E}_{\theta\sim q_l}[f(\theta)] = \frac{1}{N_\theta}\sum_{k=1}^{N_\theta} f(\theta_l^{(k)})$ and evaluate it directly.

We observe that, at each iteration, the work of each particle can be easily parallelized. When a single particle is employed, Algorithm 1 reduces to standard Newton, and the algorithm will converge to a mode of the distribution. If the Hessian in (14) is approximated by the identity matrix, Algorithm 1 coincides with Stein variational gradient descent (Liu & Wang, 2016), which in turn reduces to standard gradient descent optimization for a single particle.

Kernel and scalability. Kernel methods are known to struggle in high-dimensions (Francois et al., 2005). (Detommaso et al., 2018) shows a significant improvement in scalability by encoding second-order information in the kernel characterizing the RKHS. The following kernel is employed:

$$k(\phi,\psi) := \exp\left(-\frac{1}{2d}(\phi-\psi)^\top M(\phi-\psi)\right)\,, \tag{15}$$

where $M := \mathbb{E}_{\theta\sim q_l}[H_\pi(\theta)]$. The matrix M can be thought of as an approximation of the averaged Fisher Information, which reshapes the kernel to be a quadratic approximation of the target π, drastically improving the particle spread. We observe that M comes at no extra computation cost, since $H_\pi(\theta_l^{(k)})$ was already evaluated to perform the Newton iteration for each particle k and stage l.

The dimensional rescaling factor d in (15) attempts to reduce the increase in kernel distance as the dimensionality increases. Rescaling by d is appropriate if M is independent of d to make the ratio constant on average; alternative rescaling rates should be considered otherwise. This way, the argument of the exponential can be rescaled away from its asymptote, and the kernel's ability to discriminate between distances significantly improves in high-dimension.

2.3. SVN for BOCPD

Here we introduce SVOCD, an algorithm that generalizes BOCPD to non-exponential families of probability distributions. The $(m+1)$-th iteration of SVOCD is described in Algorithm 3, which we break down into the following steps.

Changepoint posterior update (line 3). Given samples $(\theta_{\tau_m}^{(k)})_{k=1}^{N_\theta} \sim p(\theta|Y_{\tau_m})$ and the changepoint posterior $p(\tau_m|y_{1:m-1})$ from the previous iteration, this step aims

Algorithm 1 l-th iteration of (block-diagonal) SVN

Input: Particles $(\theta_l^{(k)})_{k=1}^{N_\theta}$ at stage l; step size ε
Output: Particles $(\theta_{l+1}^{(k)})_{k=1}^{N_\theta}$ at stage $l+1$
for $k = 1, 2, \ldots, N_\theta$ **do**
    Evaluate the gradient $\nabla J_{q_l}[\mathbf{0}](\theta_l^{(k)})$ in (11)
    Evaluate the Hessian $H(\theta_l^{(k)}, \theta_l^{(k)})$ in (14)
    Solve the linear system

$$H(\theta_l^{(k)}, \theta_l^{(k)})\, Q_l(\theta_l^{(k)}) = -\nabla J_l[\mathbf{0}](\theta_l^{(k)})$$

    Update the particle

$$\theta_{l+1}^{(k)} \leftarrow \theta_l^{(k)} + \varepsilon Q_l(\theta_l^{(k)})$$

end for

Algorithm 2 Sample $y^{(i)} \sim p(y^{(i)}|y_{1:m})$

Sample $\tau^{(i)} \sim p(\tau^{(i)}|y_{1:m})$
Randomly select $\theta^{(i)}$ from $\big(\theta_{\tau^{(i)}}^{(k)}\big)_{k=1}^{N_\theta} \sim p(\theta|Y_{\tau^{(i)}})$
Sample $y^{(i)} \sim p(\cdot|Y_{\tau^{(i)}}, \theta^{(i)})$

Algorithm 3 $(m+1)$-th iteration of SVOCD

1: **Input:** $(\theta_{\tau_m}^{(k)})_{k=1}^{N_\theta}$ and $p(\tau_m|y_{1:m-1})$ for each τ_m
2: **for** $\tau_{m+1} = 1, \ldots, m+1$ **do**
3:     Evaluate $p(\tau_{m+1}|y_{1:m})$ via (16) and (3)
4:     Sample $(\theta_{\tau_{m+1}}^{(k)})_{k=1}^{N_\theta} \sim p(\theta|Y_{\tau_{m+1}})$ via Alg. 1
5: **end for**
6: Sample $(y^{(i)})_{i=1}^{N_y}$ by Alg. 2 and calculate $\bar{y}, y_\ell, y_r$
7: Observe y_{m+1} and alert changepoint if $y_{m+1} \notin [y_\ell, y_r]$

to update the changepoint posterior by the recurrent relation in (3) given the new observation y_m. We observe that this involves the evaluation of the posterior probability $p(y_m|Y_{\tau_m})$, which is a not available explicitly for a non-exponential family of probability distributions. However, because the samples $(\theta_{\tau_m}^{(k)})_{k=1}^{N_\theta}$ are available to us, we can simply estimate it by the Monte Carlo approach

$$p(y_m|Y_{\tau_m}) \approx \frac{1}{N_\theta}\sum_{k=1}^{N_\theta} p(y_m|Y_{\tau_m}, \theta_{\tau_m}^{(k)})\,. \tag{16}$$

Samples update (line 4). Next, we use SVN to generate samples $(\theta_{\tau_{m+1}}^{(k)})_{k=1}^{N_\theta} \sim p(\theta|Y_{\tau_{m+1}})$. Note that, given the changepoint τ_{m+1}, we can only have either $\tau_{m+1} = m+1$ in the case of a changepoint or $\tau_{m+1} = \tau_m$ otherwise. In the case $\tau_{m+1} = m+1$, the information set $Y_{\tau_{m+1}}$ contains no data points and, as a consequence, the posterior distribution $p(\theta|Y_{\tau_{m+1}})$ corresponds to the prior $p(\theta)$. A collection of samples $(\theta_{\tau_{m+1}}^{(k)})_{k=1}^{N_\theta}$ can now simply be taken from this prior. In the case $\tau_{m+1} = \tau_m$, we have $Y_{\tau_{m+1}} = Y_{\tau_m} \cup \{y_m\}$ which means the following decomposition holds:

$$p(\theta|Y_{\tau_{m+1}}) \propto p(y_m|Y_{\tau_m}, \theta)\, p(\theta|Y_{\tau_m})\,. \tag{17}$$

The relation in (17) shows that we can recast $p(\theta|Y_{\tau_{m+1}})$ as a sequential update of the previous posterior $p(\theta|Y_{\tau_m})$ through the information given by y_m. The transport method of SVN very well fits this framework: SVN can be initialized using the current particles $(\theta_{\tau_m}^{(k)})_{k=1}^{N_\theta} \sim p(\theta|Y_{\tau_m})$, which are then adjusted to get $(\theta_{\tau_{m+1}}^{(k)})_{k=1}^{N_\theta} \sim p(\theta|Y_{\tau_{m+1}})$. Since the initialization of the particles is optimal up to the available information Y_{τ_m}, the algorithm most likely needs only a few iterations to converge, particularly if the amount of information that y_{m+1} adds to Y_{τ_m} is small.

Data prediction (line 6). Given the updated changepoint posterior and particles, Algorithm 2 is a standard valid mechanism (Lynch, 2007) to produce samples $(y^{(i)})_{i=1}^{N_y}$ from the predictive posterior density $p(y|y_{1:m})$. We can use these samples to work out a prediction for the next observation y_{m+1} (e.g. the mean of the distribution) and statistics summarizing the distribution, for example left and right quantiles y_ℓ and y_r in the case of one-dimensional data.

Data classification (line 7). Finally, the data y_{m+1} is observed and immediately alerted as a changepoint if it does not belong to the credible interval $[y_\ell, y_r]$.

Remarks. We stress that the loops over τ_{m+1} can be executed in parallel. In particular, parallelizing the samples update step is fundamental to massively speed up the algorithm. Additional steps for pruning the set of possible values of τ_{m+1} or for optimizing over the hyper-parameters could be added (Turner et al., 2009; Wilson et al., 2010) to Algorithm 3, but this goes beyond the scope of this paper.

3. Application to Hawkes processes

In this section, we apply SVOCD to Hawkes processes: common self-exciting point processes that play a central role in analysing time series in a range of applications such as telecommunications, epidemiology, and neuroscience. Though frequentist's methods have previously been developed (Li et al., 2017; Price-Williams & Heard, 2017), this is, to the best of our knowledge, the first fully-Bayesian online treatment of detecting changepoints in Hawkes processes.

Hawkes processes. Unlike standard inhomogeneous Poisson processes, the intensity function of a self-exciting process directly depends on the occurrence of past events, which can "excite" the arrival of future events; hence the name self-exciting. In a Hawkes process, the rate of arrivals bursts whenever an event occurs, and decays over time. We denote the sequence $(y_k)_{k\geq 1}$ to be the arrival times of the process. Given that we observed the events in $Y_{\tau_{m+1}}$, the rate of arrival of the next event y_{m+1} can be described by the following *conditional intensity*:

$$\lambda_{\tau_{m+1}}(t) := \mu + \gamma \sum_{\substack{y_k \in Y_{\tau_{m+1}} \\ y_k < t}} e^{-\delta(t-y_k)}, \tag{18}$$

where $t > 0$, $\mu > 0$ is the baseline intensity rate, $\gamma > 0$ represents how much the intensity bursts whenever an event occurs, and $\delta > 0$ represents the decay rate of the intensity function. When no event has arrived yet, a Hawkes process behaves like a homogeneous Poisson process with parameter μ. We define $\theta := [\mu, \gamma, \delta]^\top$ as the 3-dimensional vector collecting all parameters. More general definitions of Hawkes processes could be considered (e.g. marked Hawkes processes, power decay functions, ...) (Rizoiu et al., 2017), but we restrict ourselves to the most common one.

Given that we observed the events in $Y_{\tau_{m+1}}$ within the time interval $(y_{\tau_{m+1}-1}, y_m]$, it can be shown that the predictive likelihood function for the next event y_{m+1} is given by

$$p(y_{m+1}|Y_{\tau_{m+1}}, \theta) = \lambda_{\tau_{m+1}}(y_{m+1})\, e^{-\Lambda_{\tau_{m+1}}\left((y_m, y_{m+1}]\right)}, \tag{19}$$

where $\Lambda_{Y_{\tau_{m+1}}}(\mathcal{I}) := \int_{\mathcal{I}} \lambda_{Y_{\tau_{m+1}}}(t)\, dt$ is known as a *compensator*, for some time interval $\mathcal{I}$ (Rasmussen, 2018). The likelihood function can then be explicitly defined as

$$p(y_{\tau_{m+1}:m}|\tau_{m+1}, \theta) = \prod_{i=\tau_{m+1}}^{m} \lambda_{\tau_{m+1}}(y_i)\, e^{-\Lambda_{\tau_{m+1}}(\mathcal{I}_{\tau_{m+1}})}, \tag{20}$$

where $\mathcal{I}_{\tau_{m+1}} := (y_{\tau_{m+1}-1}, y_m]$. In order to enforce positivity for each component of θ, we impose a log-normal prior distribution, i.e. $\ln\theta \sim \mathcal{N}(\mu_0, \sigma_0^2 I)$, where μ_0 and σ_0 are hyper-parameters. Using Bayes' Theorem, we have

$$p(\theta|Y_{\tau_{m+1}}) \propto p(y_{\tau_{m+1}:m}|\theta, \tau_{m+1})\, p(\theta). \tag{21}$$

A choice for the Hessian. In order to apply SVOCD to Hawkes processes, a positive definite approximation of the Hessian of the log-likelihood density, $\nabla_\theta^2 \log p(y_{\tau_{m+1}:m}|\tau_{m+1}, \theta)$, is required. Here, we represent this approximation by the asymptotic Fisher information, shown (Reinhart et al., 2018) to be given by

$$H_{\mathcal{L},\tau_{m+1}}(\theta) := \sum_{y_i \in Y_{\tau_{m+1}}} \nabla_\theta \log \lambda_{\tau_{m+1}}(y_i) \nabla_\theta \log \lambda_{\tau_{m+1}}(y_i)^\top. \tag{22}$$

Then, an approximation of the Hessian of the log-posterior density $\nabla_\theta^2 \log p(\theta|Y_{\tau_{m+1}})$ can be given by

$$H_{\pi,\tau_{m+1}}(\theta) = \sigma_0^2 I + H_{\mathcal{L},\tau_{m+1}}(\theta). \tag{23}$$

We note that when calculating the gradient $\nabla_\theta \log p(\theta|Y_{\tau_{m+1}})$, each $\nabla \log \lambda_{Y_{\tau_{m+1}}}(y_i)$ in (22) needs to be evaluated and hence the calculation of $H_{\pi,\tau_{m+1}}(\theta)$ does not require additional expensive operations.

Validation via SMC. To benchmark the performance of SVOCD, we also employ BOCPD using Sequential Monte Carlo (SMC) with adaptive systematic resampling (Doucet & Johansen, 2009) to update θ samples (line 4 of Algorithm 3). The importance density is taken as the Laplace approximation of the posterior density, i.e. a Gaussian centered at the MAP with covariance matrix the inverse of the Hessian evaluated at the MAP. This validation does not aim to face the difficult task of a fair performance comparison, but rather we introduce an alternative not requiring structural choices of proposal or approximating densities.

WannaCry cyber attack, 18/5/2017. WannaCry caught world headlines in May 2017 by infecting over 200,000 computers and causing damages worth at least in the hundreds of millions of dollars. The cryptoworm spread through the EternalBlue exploit on the Microsoft Windows Operating System. In this section, we consider the packet capture traffic logs of the WannaCry spread through three computers in a test environment[4]. The spread of the malware triggers a snowball effect of logs as each computer gets infected. In order to capture this self-exciting phenomena, we employ a Hawkes process to model the log arrivals in time and perform online changepoint detection to efficiently detect when the three computers become infected.

The data contains 207 time observations. The prior distribution for $\ln\theta$ was deliberately chosen as an uninformative Gaussian with parameters $\mu_0 = 0$ and $\sigma_0^2 = 10$. As we look for sudden bursts of activity, we construct a one-sided credible interval by taking y_r as the 95th percentile and we signal a changepoint m whenever $y_m > y_r$. The hazard rate in the changepoint prior and the number of predictive samples were fixed at $H_m = 100$ and $N_y = 100$, respectively.

Figure 1 displays the results of SVOCD on the WannaCry data. In the SVN algorithm, we used $N_\theta = 100$ particles and only 30 iterations. In the top figure, the horizontal axis corresponds to the index of each event, whereas the vertical axis is the actual time at which the event occurs. The blue line represents the observations. Note that a vertical jump in the data indicates that no event has occurred in that time interval, whereas horizontal regions indicate that the event arrivals were close together. The red line is the average of the predictive distribution, attempting to reconstruct the behaviour of the data; the green shadowed area represents the credibility region up to the right 95th percentile of the distribution; finally, the dashed vertical red lines are the detected changepoints. We observe that it takes some time to adapt at the very beginning of the time series, which is to be expected as the prior distribution is not yet properly tuned to the data. However, the algorithm quickly adapts and

[4]Data can be found here: https://www.malware-traffic-analysis.net/2017/05/18/index2.html.

detects three meaningful changepoints. These changepoints are also visible in the bottom figure, where we reverted the axes so that the blue line now represents a counting process which increases by 1 every time an observation occurs. We can clearly see that, apart from the initial burn-in phase, all the detected changepoints correspond to drastic bursts in activity, i.e. to the infections of the three computers. Thus, by using SVOCD we were able to identify all infections without generating any false positives (excluding burn-in).

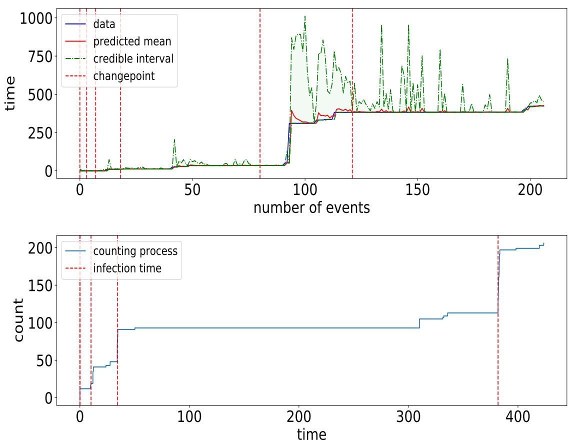

Figure 1. SVOCD with Hawkes model on WannaCry data. After burn-in, only three changepoints are detected which correspond to the infections of the three computers.

Figure 2 displays the results of BOCPD with SMC, using 1000 particles. The top figure shows that the method keeps detecting changepoints without adapting to changes in data trends. Although the bottom figure shows that these changepoints correspond to actual bursts in activity, several false positives are detected along with the machine infections.

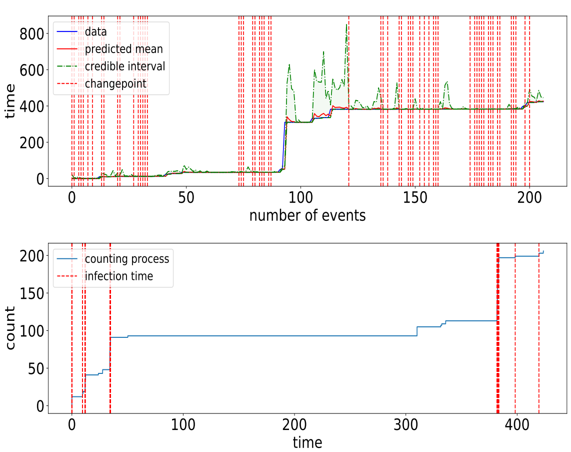

Figure 2. BOCPD + SMC with Hawkes model on WannaCry data. Several false positives are identified along the three infections.

4. Application to long short-term memory neural networks

In this section, we adopt *Bayesian long short-term memory* (BLSTM) neural networks as a predictive model for SVOCD. LSTMs have recently been applied to a large variety of scenarios because of their ability to capture temporal dynamic patterns over arbitrary time intervals. A standard description of LSTM architecture can be found in (Hochreiter & Schmidhuber, 1997; Fortunato et al., 2017; van der Westhuizen & Lasenby, 2017). We note that although frequentist's methods (Guo et al., 2016) have been proposed to detect changepoints in LSTM, this is, to the best of our knowledge, the first fully-Bayesian online changepoint analysis for LSTM. To demonstrate the effectiveness of SVOCD, we also apply BOCPD using a similar SMC method as in Section 3 to perform the parameter sampling step.

BLSTM. In the following, we will describe our Bayesian approach to LSTM. For simplicity, we use a time series of scalar data points $y_m \in \mathbb{R}$; our analysis can easily be extended to more general cases.

Consider $\mathcal{F}_{y_{\tau:m}}(\theta)$ to be the output of the forward pass of a many-to-one LSTM, trained on data $y_{\tau:m}$ and evaluated at $\theta \in \mathbb{R}^d$. The latter contains all the unknown weights and biases in the architecture of the network. If the training set of LSTM is empty, the network will just output the bias of the last layer. It is useful to also construct the corresponding many-to-many LSTM defined by $\boldsymbol{F}_{\tau:m} = [\mathcal{F}_{\emptyset}, \mathcal{F}_{y_\tau}, \mathcal{F}_{y_{\tau:\tau+1}} \dots, \mathcal{F}_{y_{\tau:m}}]$.

When $\tau = \tau_{m+1}$, the output of $\mathcal{F}_{y_{\tau_{m+1}:m}}(\theta)$ is considered a noisy prediction of the data point y_{m+1}, that is

$$y_{m+1} = \mathcal{F}_{\tau_{m+1}:m}(\theta) + \sigma\xi\,, \tag{24}$$

where $\xi \sim \mathcal{N}(0,1)$ and $\sigma > 0$. Equation (24) is equivalent to defining the predictive likelihood

$$p(y_{m+1}|Y_{\tau_{m+1}}, \theta) = \mathcal{N}(\mathcal{F}_{\tau_{m+1}:m}(\theta), \sigma^2)(y_{m+1})\,, \tag{25}$$

where the right-hand-side of (25) denotes a Gaussian density evaluated at y_{m+1} with mean $\mathcal{F}_{\tau_{m+1}:m}(\theta)$ and variance σ^2. From equation (25) and the relation between $\mathcal{F}_{\tau_{m+1}:m}$ and $\boldsymbol{F}_{\tau_{m+1}:m}$, we find that the likelihood is given by

$$p(y_{\tau_{m+1}:m}|\theta, \tau_{m+1}) = \mathcal{N}(\boldsymbol{F}_{\tau_{m+1}:m}(\theta), \sigma^2 I)(y_{\tau_{m+1}:m})\,. \tag{26}$$

Finally, we define a Gaussian prior $p(\theta) = \mathcal{N}(\mu_0, \sigma_0^2 I)$ and use Bayes' theorem as in (21) to obtain the posterior distribution.

Backprop and Fisher Information. Here, we describe how to calculate the Fisher Information of the log-likelihood, which will be used in the SVN algorithm. In deterministic LSTM, backpropagation consists of a gradient descent step which runs backwards, from the last data point to the first. In a Bayesian framework, this corresponds to calculating the gradient of the log-likelihood density:

$$\nabla \log p(y_{\tau_{m+1}:m}|\theta, \tau_{m+1}) = \frac{1}{\sigma^2} \sum_{i=\tau_{m+1}-1}^{m-1} \nabla_\theta \mathcal{F}_{\tau_{m+1}:i}(\theta)^\top (\mathcal{F}_{\tau_{m+1}:i}(\theta) - y_{i+1}) \,.$$

Given the Gaussian error assumption in (26), the Fisher Information $H_{\mathcal{L},\tau_{m+1}}$ of the likelihood is given by

$$H_{\mathcal{L},\tau_{m+1}}(\theta) := \frac{1}{\sigma^2} \sum_{i=\tau_{m+1}-1}^{m-1} \nabla_\theta \mathcal{F}_{\tau_{m+1}:i}(\theta)^\top \nabla_\theta \mathcal{F}_{\tau_{m+1}:i}(\theta) \,. \quad (27)$$

The Hessian $H_{\pi,\tau_{m+1}}$ of the log-posterior density can now be approximated as in (23).

Bitcoin price. Bitcoin is a cryptocurrency, a form of electronic cash created in 2009 whose value has fluctuated wildly in the last few years. Figure 3 shows the weekly rolling-averaged data of the evolution of bitcoin price from the beginning of 2016 to the 13th of December 2018.

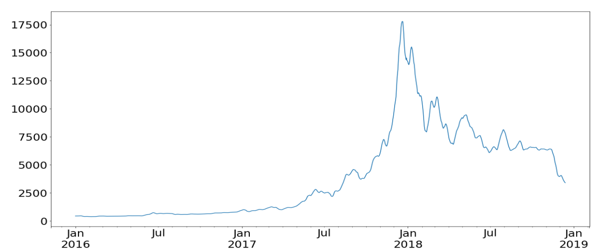

Figure 3. Bitcoin price evolution (in US dollars)

Bitcoins represent a clear case in which accurate changepoint predictions would have been very profitable. Here, we apply SVOCD with a BLSTM model to the data in Figure 3, with $\theta \in \mathbb{R}^{64}$. We use a standard Gaussian $\mathcal{N}(0, I)$ as a prior and a noise level $\sigma = 0.1$ in the likelihood. The hazard rate and the number of predictive samples were fixed at $H_m = 1000$ and $N_y = 100$, respectively.

Figure 4 shows the result of SVOCD in the region where the price dynamics reaches its all-time peak and then suddenly drops (outside this region, predictions are very stable and no changepoints are detected). Here, SVN uses $N_\theta = 30$ particles and 100 iterations. A scaled Bitcoin price is represented in blue; the red line is the mean of the predictive distribution, which tries to mimic the behaviour of the price; the green shaded area represents a 95% credible interval; finally, the vertical dashed red lines are the predicted changepoints. From December 2017, changepoints start to be detected due to the large increase in stock price. Just after the all-time peak, as soon as the price starts to decrease steeply, another changepoint is detected. Finally, various other changepoints are found corresponding to large fluctuations in price, with the last detection around the middle of February.

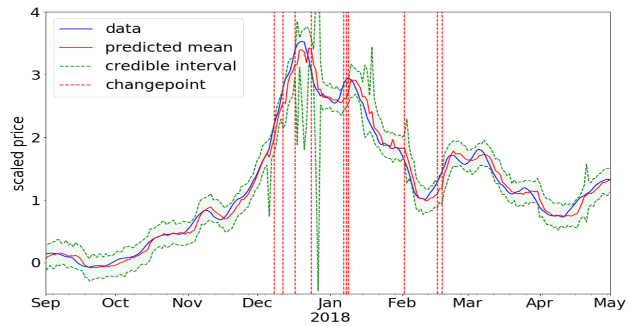

Figure 4. SVOCD with BLSTM model on Bitcoin data

In comparison, Figure 5 shows the changepoint analysis performed with BOCPD in conjunction with an SMC algorithm with 100 particles. This method detects changepoints in very similar locations as SVOCD, although the increased number of changepoints in the rising phase indicates a difficulty in adapting to changes in trend. In addition, the red predicted mean is rougher and less accurate than the one produced by SVN, despite using more particles in the simulation.

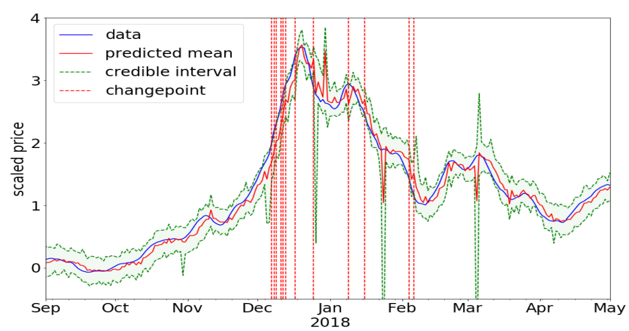

Figure 5. BOCPD + SMC with BLSTM model on Bitcoin data

5. Conclusion

In this work we introduced SVOCD, a fully-Bayesian method that combines BOCPD and SVN to detect changepoints online and accurately. We successfully applied our method to novel and challenging applications, namely Hawkes processes and LSTM neural networks on WannaCry and Bitcoin real data sets, respectively. We showed that, given the transport nature of SVN, the method is able to carry forward the current estimation of the posterior density and update it with a low number of iterations. The method is not only fast, but also accurate: because it samples from the correct posterior, it is able to quickly adapt to changes in trends, to return informative changepoints and to avoid false positives.

6. Acknowledgements

This work was fully sponsored by G-Research. We thank the InfoSecurity division of G-Research for their support. In particular, we would like to acknowledge David Thomas for facilitating the project and Antoine Vianey-Liaud for setting up the WannaCry data set.

A. SVN for Bayesian LSTM

In this section, we validate the use of SVN on a Bayesian LSTM model in order to sample correctly from a posterior distribution. In addition, we provide evidence that the prediction given by a Bayesian LSTM is substantially better than the one using a corresponding regularized LSTM.

We use the following simple test case: the data is generated by a noisy sinusoidal signal:

$$y_j = \sin(j) + \xi\,,$$

where $j = 0, \ldots, 50$ are time indices and $\xi \sim \mathcal{N}(0, 0.15^2)$ is Gaussian noise. We attempt to reconstruct the data $y_{1:50}$ and its uncertainty by using the Bayesian LSTM model described in the paper. We set a Gaussian prior $p(\theta) = \mathcal{N}(0, 1)$. We further assume a likelihood of the form $\mathcal{N}(\mathcal{F}_{1:49}(\theta), 0.3^2)$, where $\mathcal{F}_{1:49}(\theta)$ is the output of the forward pass of a many-to-many LSTM trained on $y_{1:49}$ and evaluated at parameters $\theta \in \mathbb{R}^{64}$. In order to train the BLSTM model, we use SVN with 30 particles initialized around the MAP of the distribution and run it for 100 iterations.

Figure 6 displays the results of our simulation. The blue line is the real data. The red line is the average of the particles representing our prediction. The green shaded area represents a 95% credible interval around the mean. We can see how the red prediction captures the sinusoidal motion of the signal, while the uncertainty of the signal is well represented by the green area. In contrast, the dashed magenta line is the mode of the distribution, i.e. the estimator that would be returned by a deterministic regularized LSTM. We can see very clearly that the mode of the distribution overweights the importance of the last observations: at every stage the magenta line almost exactly replicates the previous observation.

In conclusion, we find that: i) SVN is able to correctly represent the posterior distribution, and ii) a Bayesian framework is superior to a deterministic one: it allows us to calculate the average of the posterior distribution, leading to much better predictions compared to using the mode found by deterministic models.

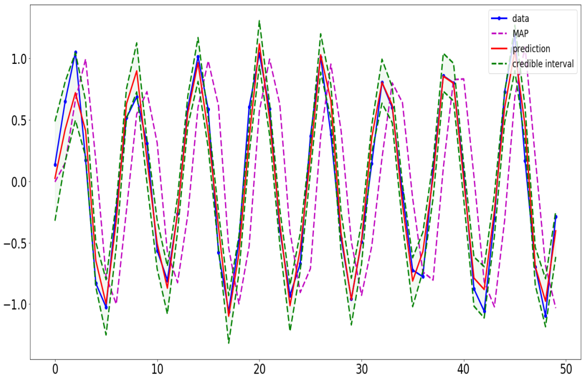

Figure 6. BLSTM trained with SVN on sinusoidal signal

References

Adams, R. P. and MacKay, D. J. Bayesian online changepoint detection. *arXiv preprint arXiv:0710.3742*, 2007.

Bacry, E., Mastromatteo, I., and Muzy, J.-F. Hawkes processes in finance. *Market Microstructure and Liquidity*, 1 (01):1550005, 2015.

Caron, F., Doucet, A., and Gottardo, R. On-line changepoint detection and parameter estimation with application to genomic data. *Statistics and Computing*, 22(2):579–595, 2012.

Dassios, A., Zhao, H., et al. Exact simulation of Hawkes process with exponentially decaying intensity. *Electronic Communications in Probability*, 18(62):1–13, 2013.

Detommaso, G., Cui, T., Marzouk, Y., Spantini, A., and Scheichl, R. A Stein variational Newton method. In *Advances in Neural Information Processing Systems*, pp. 9187–9197, 2018.

Doucet, A. and Johansen, A. M. A tutorial on particle filtering and smoothing: Fifteen years later. *Handbook of nonlinear filtering*, 12(656-704):3, 2009.

Embrechts, P., Liniger, T., and Lin, L. Multivariate Hawkes processes: an application to financial data. *Journal of Applied Probability*, 48(A):367–378, 2011.

Fearnhead, P. and Liu, Z. On-line inference for multiple changepoint problems. *Journal of the Royal Statistical Society: Series B (Statistical Methodology)*, 69(4):589–605, 2007.

Fortunato, M., Blundell, C., and Vinyals, O. Bayesian recurrent neural networks. *arXiv preprint arXiv:1704.02798*, 2017.

Francois, D., Wertz, V., Verleysen, M., et al. About the locality of kernels in high-dimensional spaces. In *International Symposium on Applied Stochastic Models and Data Analysis*, pp. 238–245. Citeseer, 2005.

Garnett, R., Osborne, M. A., and Roberts, S. J. Sequential Bayesian prediction in the presence of changepoints. In *Proceedings of the 26th Annual International Conference on Machine Learning*, pp. 345–352. ACM, 2009.

Guo, T., Xu, Z., Yao, X., Chen, H., Aberer, K., and Funaya, K. Robust online time series prediction with recurrent neural networks. In *Data Science and Advanced Analytics (DSAA), 2016 IEEE International Conference on*, pp. 816–825. Ieee, 2016.

Heard, N. A. and Turcotte, M. J. Adaptive sequential monte carlo for multiple changepoint analysis. *Journal of Computational and Graphical Statistics*, 26(2):414–423, 2017.

Hochreiter, S. and Schmidhuber, J. Long short-term memory. *Neural computation*, 9(8):1735–1780, 1997.

Lewis, E., Mohler, G., Brantingham, P. J., and Bertozzi, A. L. Self-exciting point process models of civilian deaths in Iraq. *Security Journal*, 25(3):244–264, 2012.

Li, S., Xie, Y., Farajtabar, M., Verma, A., and Song, L. Detecting changes in dynamic events over networks. *IEEE Transactions on Signal and Information Processing over Networks*, 3(2):346–359, 2017.

Liu, Q. Stein variational gradient descent as gradient flow. In *Advances in neural information processing systems*, pp. 3115–3123, 2017.

Liu, Q. and Wang, D. Stein variational gradient descent: A general purpose Bayesian inference algorithm. In *Advances In Neural Information Processing Systems*, pp. 2378–2386, 2016.

Liu, S., Yamada, M., Collier, N., and Sugiyama, M. Change-point detection in time-series data by relative density-ratio estimation. *Neural Networks*, 43:72–83, 2013.

Lynch, S. M. *Introduction to applied Bayesian statistics and estimation for social scientists*. Springer Science & Business Media, 2007.

Mavrogonatou, L. and Vyshemirsky, V. Sequential importance sampling for online Bayesian changepoint detection. In *22nd International Conference on Computational Statistics*, pp. 73–84, 2016.

Niekum, S., Osentoski, S., Atkeson, C. G., and Barto, A. G. Online Bayesian changepoint detection for articulated motion models. In *Robotics and Automation (ICRA), 2015 IEEE International Conference on*, pp. 1468–1475. IEEE, 2015.

Ogata, Y. Space-time point-process models for earthquake occurrences. *Annals of the Institute of Statistical Mathematics*, 50(2):379–402, 1998.

Price-Williams, M. and Heard, N. Statistical Modelling of Computer Network traffic event times. *arXiv preprint arXiv:1711.10416*, 2017.

Rasmussen, J. G. Lecture Notes: Temporal Point Processes and the Conditional Intensity Function. *arXiv preprint arXiv:1806.00221*, 2018.

Reinhart, A. et al. A review of self-exciting spatio-temporal point processes and their applications. *Statistical Science*, 33(3):299–318, 2018.

Rizoiu, M.-A., Lee, Y., Mishra, S., and Xie, L. A Tutorial on Hawkes Processes for Events in Social Media. *arXiv preprint arXiv:1708.06401*, 2017.

Saatçi, Y., Turner, R. D., and Rasmussen, C. E. Gaussian process change point models. In *Proceedings of the 27th International Conference on Machine Learning (ICML-10)*, pp. 927–934. Citeseer, 2010.

Turner, R., Saatci, Y., and Rasmussen, C. E. Adaptive sequential Bayesian change point detection. In *Advances in Neural Information Processing Systems: Temporal Segmentation Workshop*, 2009.

Turner, R. D., Bottone, S., and Stanek, C. J. Online variational approximations to non-exponential family change point models: with application to radar tracking. In *Advances in Neural Information Processing Systems*, pp. 306–314, 2013.

van der Westhuizen, J. and Lasenby, J. Bayesian LSTMs in medicine. *arXiv preprint arXiv:1706.01242*, 2017.

Villani, C. *Optimal transport: old and new*, volume 338. Springer Science & Business Media, 2008.

Wilson, R. C., Nassar, M. R., and Gold, J. I. Bayesian online learning of the hazard rate in change-point problems. *Neural computation*, 22(9):2452–2476, 2010.

Zhou, K., Zha, H., and Song, L. Learning social infectivity in sparse low-rank networks using multi-dimensional Hawkes processes. In *Artificial Intelligence and Statistics*, pp. 641–649, 2013.